CHAPTER-5

PULSATIONAL MODE FLUCTUATIONS AND BASIC CONSERVATION LAWS

Abstract: *In this Chapter, an inertia-centric theoretical model is proposed for investigating the basic features of nonlinear pulsational mode stability in a planar, partially ionized dust molecular cloud (DMC) within the framework of the Jeans homogenization assumption. The active inertial roles of the thermal species are included. The grain-charge is assumed not to vary in the fluctuation evolution time scale. It is shown that the electrostatic and self-gravitational eigenmodes co-exist as solitary spectral patterns governed by a pair of Korteweg–de Vries (KdV) equations relevant for such clouds. In addition, all the relevant classical conserved quantities associated with the constructed KdV system under translational invariance are methodologically derived and numerically analyzed. It is demonstrated that the solitary mass, momentum and energy densities also evolve like solitary spectral patterns, but with different characteristic features discussed here, which remain conserved throughout the spatiotemporal scales of the fluctuation dynamics. Astrophysical and space environments relevant to the findings are briefly highlighted.*

5.1 INTRODUCTION

In the interstellar medium, the gravito-electrostatic coupling of partially-ionized self-gravitating dust molecular cloud (DMC) is responsible for tremendous amount of energy through star formation processes [1-4]. The source of free energy for this gravito-electrostatic instability lies in the associated self-gravity of the dispersed phase of the dust grains of solid matter over the gaseous phase of the background plasma. Such type of instability occurs when the self-gravitational collapsing force exceeds the collective repulsive forces of the cloud, and gives rise to different types of nonlinear eigenmodes [1-5]. These nonlinear eigenmodes ultimately produce the initial conditions for diverse stellar, planetary, and galactic structure formations [1-8].

It may be seen that, there have been many earlier waves, oscillations, and stability analyses on various grainy plasma systems in diverse space and astrophysical situations as reported by different researchers [1-9]. It has also been found that when the coupling between the neutral fluid and the plasma is considered, a new short wavelength electromagnetic mode (Jeans-type) is excited

in the self-gravitating magnetoplasma [7]. It has been suggested that such new instabilities could be responsible for the fragmentation of the cloud into sub-structures collapsing to form the stars and other astrophysical objects [7-8]. But, nobody has so far addressed the fluctuation eigenmodes in presence of the weak but finite inertial effects of the plasma thermal species. Even in presence of the massive grains, the lowest-order inertia of the thermal species has been found to possess a unique quality of destabilizing the normal plasma mode in uniform flow region [9]. Besides, the conservative nature of the gravito-electrostatic nonlinear fluctuations in diverse astrophysical situations is also yet to be well understood.

In this chapter, we develop a systematic methodology to demonstrate a full existence of new nonlinear eigenmode features of gravito-electrostatic significance in an infinite self-gravitating inhomogeneous cloud (Cartesian 1-D geometry) with all the possible realistic collisional effects [1-4, 10-11] taken into account in hydrodynamic equilibrium configuration. In addition, this includes the lowest-order inertial correction [9, 12] of the thermal species. Applying a standard multiscale analysis over the defined cloud equilibrium, it is shown that the electrostatic and self-gravitational eigenmodes evolve as diverse solitary spectral patterns governed by a pair of gravito-electrostatically coupled Korteweg–de Vries (KdV) type equations. A full numerical shape-analysis of the fluctuations with multi-parameter variation of judicious plasma conditions is also carried out to study the internal microphysics of the spectral patterns. Moreover, the KdV system is well-known as a conservative integrable model possessing an infinite string of conservation laws [13-14]. So, motivated by the conservative features of the fluctuations, we, analytically derive different basic conservative forms of the pulsational KdV dynamics. The evolutionary patterns of all the associated relevant conserved quantities are numerically analyzed. Interestingly, we find a unique property that the dynamical evolution of the mass density, momentum density, and energy density of the lowest-order gravito-electrostatic potential fluctuations retain the shape of soliton-like patterns in all the cases.

5.2 PHYSICAL MODEL

A simplified astrophysical situation of a self-gravitating DMC within the framework of planar (1-D) geometry approximation in hydrodynamic equilibrium on the Jeans scale is considered. Such a geometrical model may justifiably have a spherical symmetry, but in the radial (1-D) direction only. The global quasi-neutrality in the presence of convective nonlinearity and neutral-charged

grain collisional dynamics is taken into account. It could be visualized as a static distribution of the multi-fluid consisting of the electrons, ions, neutral gas, and identical dust grains with partial ionization. The thermal electrons and ions are assumed to have weak inertia, and the massive grains are fully inertial in nature. The considered dust grains get negatively charged (for $v_{te} >> v_{ti}$) through various attachment phenomena due to the plasma environment amid statistically random collision processes with the thermal species [3-4, 10-11]. The grain charging mechanism is a dynamic process in which the background electrons and ions are collected spontaneously. We consider a steady-state configuration of the identical charged grains, which means that the charge does not vary during the fluctuation evolution of interest [3-4, 10-11]. In fact, such self-gravitating plasmas are inhomogeneous in nature [3, 10-11, 15]. However, for simplification, our model is methodologically developed based on the Jeans assumption of self-gravitating uniform homogenous plasma [10, 15]. Thus, the zeroth-order self-gravitational field is neglected, and the equilibrium is treated initially as 'homogeneous', thereby validating local analysis.

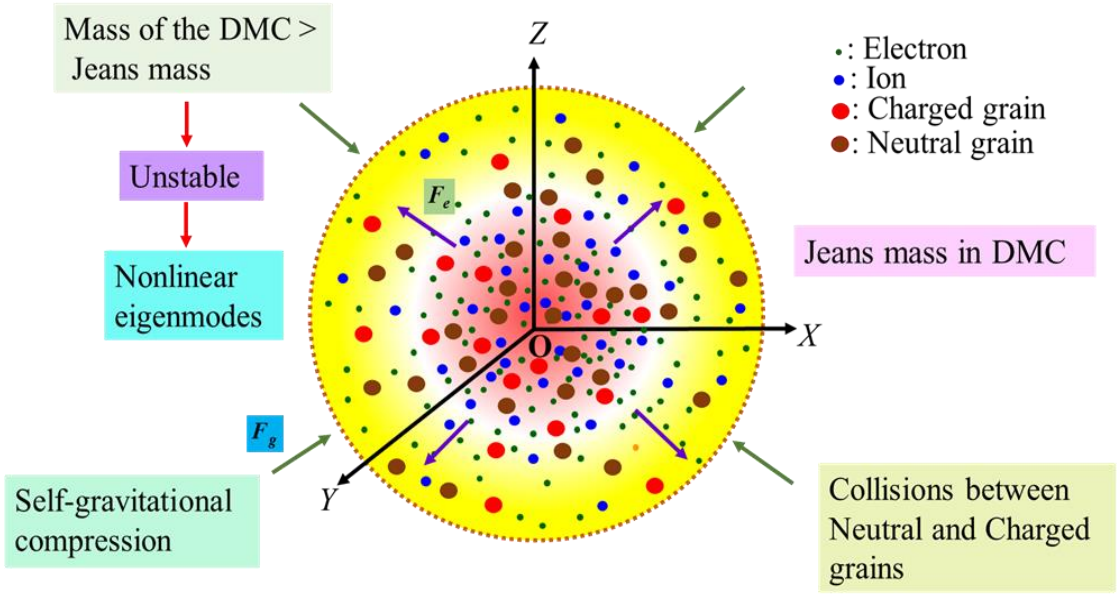

Figure 5.1 *Schematic diagram showing a partially ionized DMC model.*

In normal DMCs, magnetic field is $\sim 1\mu G$ [10], around which the charged grains, in principle, perform gyration [1]. For $q_d \sim 100e$, and $m_d \sim 10^{-13}$ kg [1, 4], the gyro-period of the grains is $\tau_{cd} \sim 10^6$ years, which is too slow to influence the grainy dynamics considerably. The effects of

the magnetic field on the grains are experienced through plasma particles, which are usually well coupled to the field. So, the effect of the magnetic field is ignored, and an unmagnetized cloud configuration [1] is considered. The drag effects and other force field effects are also neglected for the time being. For simplicity, we ignore complications like dust-charge fluctuation, grain size-distribution, rotation, viscosity, spatiotemporal inhomogeneities, etc.

Figure 5.1 pictorially shows the morphology of a partially ionized DMC. The efficacious inertial mass of the cloud is collectively contributed by the heavier grains, and negligibly by the inertia-corrected thermal species, but it is valid within the limit of Newtonian point-mass approximation. An assumed wide-range spectrum in the grain-mass ($m_d \sim 10^{-9} - 10^{-21}$ kg) physically allows a suitable parameter regime, where, the monopolar self-gravitational (F_g) and bipolar electrostatic forces (F_e) may become approximately comparable. Thus, if the grain charge-to-mass ratio is such that $Gm_d^2 / q_d^2 \sim 0(1)$, the joint interplayed action of the two opposing forces in establishing gravito-electrostatic equilibrium may play an important role in the formation processes of equilibrium stellar structures. It may further be worth mentioning that the adopted model setup sustains the nonlinearity (wave steepening agency) due to fluidity, the dispersion (wave spreading agency) due to self-gravitational interaction within the planar geometry, and the dissipation (wave damping agency) because of collective collisional dynamics of intrinsic cloud origin [11]. The strength of the electric forces developed from space-charge polarization effects (local charge imbalance) are considered to be too weak to excite higher order contributions of various nonlinear terms, thereby validating our underlying assumption of weak nonlinearity.

5.3 MATHEMATICAL FORMULATION

We are interested to investigate the nonlinear electro-gravitational stability of the pulsational mode dynamics in presence of the inertia-corrected thermal electrons and ions, and their basic conservation laws. So, the lowest-order inertia-corrected normalized densities with all conventional notations described later [9, 12] for the electrons and ions can be written as follows,

$$N_e = exp\left[\left(\frac{1}{2}\right)\frac{m_e}{m_i} M_{eo}^2 \{1 - exp(-2\Phi)\} + \Phi\right], \text{ and} \tag{5.1}$$

$$N_i = exp\left[\left(\frac{1}{2}\right)\frac{m_i}{m_d} M_{io}^2 \{1 - exp(2\Phi)\} - \Phi\right]. \tag{5.2}$$

Thus, the equations (5.1)-(5.2) contains the lowest-order inertial characteristics through the presence of inertial correction factor m_e/m_i and m_i/m_d (asymptotic electron-to-ion and ion-to-dust mass ratios), respectively. The normalized equations governing the dynamics of the neutral and charged dust within the framework of the Jeans homogenization assumption [1, 10, 15] are

$$\frac{\partial N_s}{\partial \tau} + N_s \frac{\partial M_s}{\partial \xi} + M_s \frac{\partial N_s}{\partial \xi} = 0, \tag{5.3}$$

$$\frac{\partial M_s}{\partial \tau} + M_s \frac{\partial M_s}{\partial \xi} = -\chi \frac{\partial \Phi}{\partial \xi} - \left(\frac{m_d}{e}\right)\frac{\partial \Psi}{\partial \xi} - f, \tag{5.4}$$

Here, the label $s = (dn, dc)$ characterizes the neutral and charged grain species. For $s = dn$, one has $\chi = 0$, and $f = 0$. Similarly, for $s = dc$, we have $\chi = q_d/e$, and $f = F_{cn}(M_{dc} - M_{dn})$. The spatial distributions of the normalized electrostatic potential (Φ), and self-gravitational potential (Ψ) are described by the combining Poisson equations thereby closing the model as given below,

$$\frac{\partial^2 \Phi}{\partial \xi^2} = \frac{4\pi e^2}{m_d \omega_J^2}\left\{n_{eo}N_e - n_{io}N_i - \left(n_{dco}\frac{q_d}{e}\right)N_{dc}\right\}, \text{ and} \tag{5.5}$$

$$\frac{\partial^2 \Psi}{\partial \xi^2} = \frac{4\pi G e}{\omega_J^2}\left\{n_{dco}N_{dc} + n_{dno}N_{dn} - n_{do}N_{do} + \left(\frac{m_e}{m_d}\right)n_{eo}N_e + \left(\frac{m_i}{m_d}\right)n_{io}N_i\right\}. \tag{5.6}$$

All the astrophysical self-gravitating clouds are inhomogeneous in nature. But, analytically dealing with an inhomogeneous equilibrium configuration is too complicated. So, to make it simpler, we use $n_{do} = n_{dco} + n_{dno}$ in equation (5.6), which models the Jeans swindle [10, 15] of the equilibrium unipolar gravitational force field. It provides a formal justification that the self-gravitational potential is sourced only by density fluctuations of the infinite uniform homogeneous medium. Usually, the Jeans assumption for self-gravitating homogeneous medium is not so realistic, but for simplicity of analytical calculation, it allows us to treat the complicated inhomogeneous plasma dynamics as 'homogeneous' one [10, 15]. All the notations used above are generic and usual. The parameters $M_{dn}(\xi)$, $M_{dc}(\xi)$, $\Phi(\xi)$, and $\Psi(\xi)$ represent the normalized neutral dust flow velocity, charged dust flow velocity, electrostatic and self-gravitational potentials, respectively. The velocities are normalized by the dust sound phase speed (C_{SS}), and the potentials are normalized by the cloud thermal potential (T_p/e). The independent variables like space (ξ), and time (τ) are normalized by the Jeans length (λ_J), and Jeans time (ω_J^{-1}) scales, respectively. Moreover, N_e,

N_i, N_{dn}, and N_{dc} are the population densities of the electrons, ions, neutral, and charged grains normalized by their respective equilibrium densities n_{eo}, n_{io}, n_{dno}, and n_{dco}, respectively. Furthermore, F_{cn} is the charged-neutral grain collision frequency normalized by the Jeans frequency ω_J. The notations m_e, m_i, and m_d denote the mass of the electrons, ions, and the dust grains with temperature T_e, T_i, and T_d; equilibrium flow M_{eo}, M_{io}, M_{dco}; and charge $-e$, $+e$ and q_d; respectively, where $T_d << T_e \approx T_i = T_p$ (in eV).

We apply a standard methodology of multiscale analysis [16] over the equations (5.1)-(5.6) around the zeroth-order homogeneous configuration in a new stretched space defined by the transformations $X = \in^{1/2}(\xi - \mu\tau)$, and $T = \in^{3/2}\tau$ [16], where $\in$ is a minor parameter characterizing the balanced strength of nonlinearity and dispersion, and μ is the phase velocity (normalized by C_{ss}) of the fluctuations. The dependent variables like densities, potentials, and velocities in equations (5.1)-(5.6) are now expanded nonlinearly (in $\in$-powers) around the respective equilibrium values of the defined equilibrium dust cloud as follows,

$$\begin{pmatrix} N_e(\xi,\tau) \\ N_i(\xi,\tau) \\ N_s(\xi,\tau) \\ M_s(\xi,\tau) \\ \Phi(\xi,\tau) \\ \Psi(\xi,\tau) \end{pmatrix} = \begin{pmatrix} 1 \\ 1 \\ 1 \\ 0 \\ 0 \\ 0 \end{pmatrix} + \in \begin{pmatrix} N_{e1}(\xi,\tau) \\ N_{i1}(\xi,\tau) \\ N_{s1}(\xi,\tau) \\ M_{s1}(\xi,\tau) \\ \Phi_1(\xi,\tau) \\ \Psi_1(\xi,\tau) \end{pmatrix} + \in^2 \begin{pmatrix} N_{e2}(\xi,\tau) \\ N_{i2}(\xi,\tau) \\ N_{s2}(\xi,\tau) \\ M_{s2}(\xi,\tau) \\ \Phi_2(\xi,\tau) \\ \Psi_2(\xi,\tau) \end{pmatrix} + \cdots\cdots, \tag{5.7}$$

In our model, the gravity-induced electric polarization effects are neglected for mathematical simplicity as discussed elaborately in chapter 4. We use equation (5.7) over equations (5.1)-(5.6) and after order-by-order analyses (in $\in$-powers) with systematic rigorous calculations; we finally obtain electrostatic and self-gravitational Korteweg de–Vries (KdV) equations to study the gravito-electrostatic fluctuations of the cloud. Accordingly, the electrostatic fluctuations are governed by,

$$\frac{\partial \Phi_1}{\partial T} + \beta_1 \Phi_1 \frac{\partial \Phi_1}{\partial X} + \beta_2 \frac{\partial^3 \Phi_1}{\partial X^3} = 0 \ , \tag{5.8}$$

which is the electrostatic KdV equation with coefficients $\beta_1 = \alpha_2/\alpha_1$, and $\beta_2 = \alpha_3/\alpha_1$, where,

$$\alpha_1 = \left[\frac{1}{(M_{dco} - M_{dno})} \left(\frac{e^2}{m_d^2 G n_{dno}} \right) A_1 + \frac{N_{dno}}{(M_{dno} - \mu)^2 (M_{dno} - M_{dco})} \left(\frac{q_d^2}{m_d^2 G} \right) \right], \tag{5.9}$$

$$\alpha_2 = \left[Z_d \frac{2N_{dno}}{(M_{dno}-\mu)^2 (M_{dco}-M_{dno})^2} \left(\frac{q^2}{m_d^2 G} \right) - \frac{Z_d}{(M_{dno}-M_{dco})^2} \left(\frac{e^2}{m_d^2 G n_{dno}} \right) A_1 \right], \tag{5.10}$$

$$\alpha_3 = \left[\left\{ \left(\frac{q_d}{m_d} \right)^2 \frac{1}{G} \left(\frac{\mu - M_{dno}}{M_{dco}-M_{dno}} \right) \right\} - 1 \right], \text{ and} \tag{5.11}$$

$$A_1 = \left[\left\{ n_{eo} \left(1 + Z_d \frac{m_e}{m_d} \right) \left(1 + \left(\frac{m_e}{m_i} \right) M_{eo}^2 e^{(-2\Phi_o)} \right) \right\} + \left\{ n_{io} \left(-1 + Z_d \frac{m_i}{m_d} \right) \left(-1 - \left(\frac{m_i}{m_d} \right) M_{io}^2 e^{(2\Phi_o)} \right) \right\} \right]. \tag{5.12}$$

The self-gravitational fluctuations are governed by,

$$\frac{\partial \Psi_1}{\partial T} + \Theta_1 \Psi_1 \frac{\partial \Psi_1}{\partial X} + \Theta_2 \frac{\partial^3 \Psi_1}{\partial X^3} = 0, \tag{5.13}$$

which is self-gravitational KdV equation with coefficients $\Theta_1 = \chi_2/\chi_1$, and $\Theta_2 = \chi_3/\chi_1$, such that,

$$\chi_1 = \left[\left\{ \frac{N_{dno}}{(\mu - M_{dno})^3} \right\} + \left\{ \frac{e}{q_q n_{dno} (M_{dno} - \mu)} \right\} A_2 \right], \tag{5.14}$$

$$\chi_2 = \left[\left\{ \frac{2N_{dno} m_d}{e(\mu - M_{dno})^4} \right\} - \left\{ \frac{m_d}{q_d n_{dno} (\mu - M_{dno})^2} \right\} A_2 \right], \tag{5.15}$$

$$\chi_3 = \left[\left\{ \frac{m_d^2 G (M_{dco} - M_{dno})}{q_d^2 (\mu - M_{dno})} \right\} - 1 \right], \text{ and} \tag{5.16}$$

$$A_2 = \left[\left(1 + \left(\frac{m_e}{m_i} \right) M_{eo}^2 e^{(-2\Phi_o)} \right) n_{eo} \left(\frac{1}{Z_d} + \frac{m_e}{m_d} \right) + \left(-1 - \left(\frac{m_i}{m_d} \right) M_{io}^2 e^{(2\Phi_o)} \right) n_{io} \left(\frac{m_i}{m_d} - \frac{1}{Z_d} \right) \right]. \tag{5.17}$$

We are interested in the basic features of the steady-state structures of the fluctuation dynamics. So, equations (5.8) and (5.13) are transformed into ordinary differential equations (ODEs) by the Galilean co-moving transformation $\rho = X - T$, and given by

$$\frac{\partial \Phi_1}{\partial \rho} - \beta_1 \Phi_1 \frac{\partial \Phi_1}{\partial \rho} - \beta_2 \frac{\partial^3 \Phi_1}{\partial \rho^3} = 0, \text{ and} \tag{5.18}$$

$$\frac{\partial \Psi_1}{\partial \rho} - \Theta_1 \Psi_1 \frac{\partial \Psi_1}{\partial \rho} - \Theta_2 \frac{\partial^3 \Psi_1}{\partial \rho^3} = 0. \tag{5.19}$$

Equations (5.18)-(5.19) together constitute a unique steady-state pair KdV equations in a new space coordinatized by ρ, which show the fluctuations supported in the partially-ionized DMC.

5.4. CONSERVATION LAWS

The KdV type nonlinear systems are well-known to possess an infinite string of conserved quantities due to its property of complete integrability [13-14]. Many authors in the past have worked on the conservation laws of the KdV type equations to derive the explicit form of the associated conserved densities and corresponding flux-forms. They have shown that autonomous evolution equations with translation invariance have three physically significant basic conserved quantities, such as mass, momentum, and energy [13-14]. So, we are motivated to see the evolution nature of the conserved quantities of the cloud by applying the same strategy. Accordingly, we derive the basic conserved quantities of our gravito-electrostatic KdV dynamics as follows.

5.4.1 Conservative forms of Electrostatic KdV Dynamics

The electrostatic KdV equation (5.8) can be written in a conservative form [13] as follows.

$$\frac{\partial P_{e1}}{\partial T} + \frac{\partial Q_{e1}}{\partial X} = 0, \tag{5.20}$$

where,

$$P_{e1} = \Phi_1, \text{ and} \tag{5.21}$$

$$Q_{e1} = \frac{1}{2}\beta_1 \Phi_1^2 + \beta_2 \frac{\partial^2 \Phi_1}{\partial X^2}. \tag{5.22}$$

Equations (5.21) and (5.22) give conserved mass density of electrostatic soliton and associated mass flux governed by the dynamical evolution of the system, respectively [13]. Equation (5.8) is multiplied by Φ_1 (with rank 1) [13], and associated corresponding conservative form is written as,

$$\frac{\partial P_{e2}}{\partial T} + \frac{\partial Q_{e2}}{\partial X} = 0, \tag{5.23}$$

where,

$$P_{e2} = \frac{1}{2}\Phi_1^2, \text{ and} \tag{5.24}$$

$$Q_{e2} = \frac{1}{3}\beta_1 \Phi_1^3 + \beta_2 \Phi_1 \frac{\partial^2 \Phi_1}{\partial X^2} - \frac{1}{2}\beta_2 \left(\frac{\partial \Phi_1}{\partial X}\right)^2. \tag{5.25}$$

Equation (5.24) gives the conserved momentum density and equation (5.25) gives associated momentum flux of the electrostatic KdV solitary structure. Again, equation (5.8) is multiplied by Φ_1^2 (with rank 2) [13] and associated conservative form is presented as,

$$\frac{\partial P_{e3}}{\partial T}+\frac{\partial Q_{e3}}{\partial X}=0, \tag{5.26}$$

where,

$$P_{e3}=\frac{1}{3}\beta_1\Phi_1^3-\beta_2\left(\frac{\partial\Phi_1}{\partial X}\right)^2, \text{ and} \tag{5.27}$$

$$Q_{e3}=\frac{1}{4}\beta_1^2\,\Phi_1^4+\beta_1\beta_2\Phi_1^2\frac{\partial^2\Phi_1}{\partial X^2}-2\beta_1\beta_2\Phi_1\left(\frac{\partial\Phi_1}{\partial X}\right)^2-2\beta_2^2\frac{\partial\Phi_1}{\partial X}\frac{\partial^3\Phi_1}{\partial X^3}+\beta_2^2\left(\frac{\partial^2\Phi_1}{\partial X^2}\right)^2. \tag{5.28}$$

Thus, equation (5.27) gives the conserved energy density and equation (5.28) provides the associated energy flux of the electrostatic KdV equation [13]. Similarly, we get the higher-order conserved quantities and conserved flux of the electrostatic KdV soliton respectively as follows,

$$P_{e4}=\frac{1}{4}\beta_1\Phi_1^4-3\beta_2\Phi_1\left(\frac{\partial\Phi_1}{\partial X}\right)^2+\frac{9}{5}\frac{\beta_2^2}{\beta_1}\left(\frac{\partial^2\Phi_1}{\partial X^2}\right)^2, \tag{5.29}$$

$$\begin{aligned}Q_{e4}=&\frac{1}{5}\beta_1^2\,\Phi_1^5+\beta_1\beta_2\Phi_1^3\frac{\partial^2\Phi_1}{\partial X^2}-\frac{9}{2}\beta_1\beta_2\Phi_1^2\left(\frac{\partial\Phi_1}{\partial X}\right)^2-6\beta_2^2\Phi_1\frac{\partial\Phi_1}{\partial X}\frac{\partial^3\Phi_1}{\partial X^3}-\frac{9}{5}\frac{\beta_2^3}{\beta_1}\left(\frac{\partial^3\Phi_1}{\partial X^3}\right)^2\\&+\frac{24}{5}\beta_2^2\Phi_1\left(\frac{\partial^2\Phi_1}{\partial X^2}\right)^2+3\beta_2^2\left(\frac{\partial\Phi_1}{\partial X}\right)^2\frac{\partial^2\Phi_1}{\partial X^2}+\frac{18}{5}\frac{\beta_2^3}{\beta_1}\frac{\partial^2\Phi_1}{\partial X^2}\frac{\partial^4\Phi_1}{\partial X^4};\end{aligned} \tag{5.30}$$

$$P_{e5}=\frac{1}{5}\beta_1\Phi_1^5-6\beta_2\Phi_1^2\left(\frac{\partial\Phi_1}{\partial X}\right)^2+\frac{36}{5}\frac{\beta_2^2}{\beta_1}\Phi_1\left(\frac{\partial^2\Phi_1}{\partial X^2}\right)^2-\frac{108}{35}\frac{\beta_2^3}{\beta_1^2}\left(\frac{\partial^3\Phi_1}{\partial X^3}\right)^2, \text{ and} \tag{5.31}$$

$$\begin{aligned}Q_{e5}=&\frac{1}{6}\beta_1^2\,\Phi_1^6+\beta_1\beta_2\Phi_1^4\frac{\partial^2\Phi_1}{\partial X^2}-8\beta_1\beta_2\Phi_1^3\left(\frac{\partial\Phi_1}{\partial X}\right)^2+\frac{66}{5}\beta_2^2\Phi_1^2\left(\frac{\partial^2\Phi_1}{\partial X^2}\right)^2-12\beta_2^2\Phi_1^2\frac{\partial\Phi_1}{\partial X}\\&\frac{\partial^3\Phi_1}{\partial X^3}+12\beta_2^2\Phi_1\left(\frac{\partial\Phi_1}{\partial X}\right)^2\frac{\partial^2\Phi_1}{\partial X^2}-3\beta_2^2\left(\frac{\partial\Phi_1}{\partial X}\right)^4+\frac{72}{5}\frac{\beta_2^3}{\beta_1}\Phi_1\frac{\partial^2\Phi_1}{\partial X^2}\frac{\partial^4\Phi_1}{\partial X^4}-\frac{72}{7}\frac{\beta_2^3}{\beta_1}\Phi_1\left(\frac{\partial^3\Phi_1}{\partial X^3}\right)^2\\&-\frac{72}{5}\frac{\beta_2^3}{\beta_1}\frac{\partial\Phi_1}{\partial X}\frac{\partial^2\Phi_1}{\partial X^2}\frac{\partial^3\Phi_1}{\partial X^3}+\frac{36}{35}\frac{\beta_2^3}{\beta_1}\left(\frac{\partial^2\Phi_1}{\partial X^2}\right)^3-\frac{216}{35}\frac{\beta_2^4}{\beta_1^2}\frac{\partial^3\Phi_1}{\partial X^3}\frac{\partial^5\Phi_1}{\partial X^5}+\frac{108}{5}\frac{\beta_2^4}{\beta_1^2}\left(\frac{\partial^4\Phi_1}{\partial X^4}\right)^2;\end{aligned} \tag{5.32}$$

and so forth. Thus, by repeating the above procedure, it is possible to get an infinitely large number of conserved quantities associated with the electrostatic KdV soliton.

5.3.2 Conservative forms of Self-gravitational KdV Dynamics

The self-gravitational KdV equation (5.13) can also be written in a conservative form [13] as

$$\frac{\partial P_{g1}}{\partial T}+\frac{\partial Q_{g1}}{\partial X}=0, \tag{5.33}$$

where,

$$P_{g1}=\Psi_1, \text{ and} \tag{5.34}$$

$$Q_{g1}=\frac{1}{2}\Theta_1\Psi_1^2+\Theta_2\frac{\partial^2\Psi_1}{\partial X^2}. \tag{5.35}$$

Equation (5.34) gives the conserved mass density and equation (5.35) offers the associated mass flux of the self-gravitational KdV equation. As in case of electrostatic fluctuations, here equation (5.13) is multiplied by Ψ_1 (with rank 1) [13] and associated conservative form is written as,

$$\frac{\partial P_{g2}}{\partial T}+\frac{\partial Q_{g2}}{\partial X}=0, \tag{5.36}$$

where,

$$P_{g2}=\frac{1}{2}\Psi_1^2, \text{ and} \tag{5.37}$$

$$Q_{g2}=\frac{1}{3}\Theta_1\Psi_1^3+\Theta_2\Psi_1\frac{\partial^2\Psi_1}{\partial X^2}-\frac{1}{2}\Theta_2\left(\frac{\partial\Psi_1}{\partial X}\right)^2. \tag{5.38}$$

It is clear that equation (5.37) gives the conserved momentum density and equation (5.38) gives the associated corresponding momentum flux of the self-gravitational KdV equation [13]. Again, equation (5.13) is multiplied by Ψ_1^2 (with rank 2) and associated conservative form is written as,

$$\frac{\partial P_{g3}}{\partial T}+\frac{\partial Q_{g3}}{\partial X}=0, \tag{5.39}$$

where,

$$P_{g3}=\frac{1}{3}\Theta_1\Psi_1^3-\Theta_2\left(\frac{\partial\Psi_1}{\partial X}\right)^2, \text{ and} \tag{5.40}$$

$$Q_{g3}=\frac{1}{4}\Theta_1^2\Psi_1^4+\Theta_1\Theta_2\Psi_1^2\frac{\partial^2\Psi_1}{\partial X^2}-2\Theta_1\Theta_2\Psi_1\left(\frac{\partial\Psi_1}{\partial X}\right)^2-2\Theta_2^2\frac{\partial\Psi_1}{\partial X}\frac{\partial^3\Psi_1}{\partial X^3}+\Theta_2^2\left(\frac{\partial^2\Psi_1}{\partial X^2}\right)^2. \tag{5.41}$$

Equation (5.40) gives the conserved energy density and equation (5.41) shows the associated energy flux of the self-gravitational KdV soliton. Similarly, applying the above procedure repeatedly, one gets the next higher-order conserved quantities as follows.

$$P_{g4}=\frac{1}{4}\Theta_1\Psi_1^4-3\Theta_2\Psi_1\left(\frac{\partial\Psi_1}{\partial X}\right)^2+\frac{9}{5}\frac{\Theta_2^2}{\Theta_1}\left(\frac{\partial^2\Psi_1}{\partial X^2}\right)^2, \tag{5.42}$$

$$Q_{g4}=\frac{1}{5}\Theta_1^2\Psi_1^5+\Theta_1\Theta_2\Psi_1^3\frac{\partial^2\Psi_1}{\partial X^2}-\frac{9}{2}\Theta_1\Theta_2\Psi_1^2\left(\frac{\partial\Psi_1}{\partial X}\right)^2-6\Theta_2^2\Psi_1\frac{\partial\Psi_1}{\partial X}\frac{\partial^3\Psi_1}{\partial X^3}-\frac{9}{5}\frac{\Theta_2^3}{\Theta_1}\left(\frac{\partial^3\Psi_1}{\partial X^3}\right)^2$$
$$+\frac{24}{5}\Theta_2^2\Psi_1\left(\frac{\partial^2\Psi_1}{\partial X^2}\right)^2+3\Theta_2^2\left(\frac{\partial\Psi_1}{\partial X}\right)^2\frac{\partial^2\Psi_1}{\partial X^2}+\frac{18}{5}\frac{\Theta_2^3}{\Theta_1}\frac{\partial^2\Psi_1}{\partial X^2}\frac{\partial^4\Psi_1}{\partial X^4}; \tag{5.43}$$

$$P_{g5}=\frac{1}{5}\Theta_1\Psi_1^5-6\Theta_2\Psi_1^2\left(\frac{\partial\Psi_1}{\partial X}\right)^2+\frac{36}{5}\frac{\Theta_2^2}{\Theta_1}\Psi_1\left(\frac{\partial^2\Psi_1}{\partial X^2}\right)^2-\frac{108}{35}\frac{\Theta_2^3}{\Theta_1^2}\left(\frac{\partial^3\Psi_1}{\partial X^3}\right)^2, \text{ and} \tag{5.44}$$

$$Q_{g5}=\frac{1}{6}\Theta_1^2\Psi_1^6+\Theta_1\Theta_2\Psi_1^4\frac{\partial^2\Psi_1}{\partial X^2}-8\Theta_1\Theta_2\Psi_1^3\left(\frac{\partial\Psi_1}{\partial X}\right)^2+\frac{66}{5}\Theta_2^2\Psi_1^2\left(\frac{\partial^2\Psi_1}{\partial X^2}\right)^2-12\Theta_2^2\Psi_1^2\frac{\partial\Psi_1}{\partial X}$$
$$\frac{\partial^3\Psi_1}{\partial X^3}+12\Theta_2^2\Psi_1\left(\frac{\partial\Psi_1}{\partial X}\right)^2\frac{\partial^2\Psi_1}{\partial X^2}-3\Theta_2^2\left(\frac{\partial\Psi_1}{\partial X}\right)^4+\frac{72}{5}\frac{\Theta_2^3}{\Theta_1}\Psi_1\frac{\partial^2\Psi_1}{\partial X^2}\frac{\partial^4\Psi_1}{\partial X^4}-\frac{72}{7}\frac{\Theta_2^3}{\Theta_1}\Psi_1\left(\frac{\partial^3\Psi_1}{\partial X^3}\right)^2 \tag{5.45}$$
$$-\frac{72}{5}\frac{\Theta_2^3}{\Theta_1}\frac{\partial\Psi_1}{\partial X}\frac{\partial^2\Psi_1}{\partial X^2}\frac{\partial^3\Psi_1}{\partial X^3}+\frac{36}{35}\frac{\Theta_2^3}{\Theta_1}\left(\frac{\partial^2\Psi_1}{\partial X^2}\right)^3-\frac{216}{35}\frac{\Theta_2^4}{\Theta_1^2}\frac{\partial^3\Psi_1}{\partial X^3}\frac{\partial^5\Psi_1}{\partial X^5}+\frac{108}{5}\frac{\Theta_2^4}{\Theta_1^2}\left(\frac{\partial^4\Psi_1}{\partial X^4}\right)^2;$$

and so on. Consequently, by repeating the above procedure, it is possible to get an infinitely large number of conservation laws associated with the dynamics of the self-gravitational KdV solitary spectral patterns supported in the considered cloud.

5.5 RESULTS AND DISCUSSIONS

A simplified inertia-based theoretical model is proposed to analyze the pulsational mode fluctuations in a 1-D inhomogeneous partially ionized DMC with conservative flow dynamics and neutral-charged dust collisional effects on the Jeans scales of space and time. The associated basic conservation laws are also investigated in detail. Analytical, graphical, and numerical techniques are applied for the investigation. But for simplification due to complicated large-scale dynamics, our model is methodologically developed, based on the Jeans homogenization assumption (Jeans swindle) of self-gravitating uniform homogenous plasma [10, 15]. Based on a time-stationary framework, we successfully depict a rich variety of detailed fluctuations, wave-like activities, and their parametric evolution methodologically as discussed in detail below.

5.5.1 Electrostatic Fluctuations

It is seen that electrostatic fluctuation dynamics of the self-gravitating DMC is collectively governed by electrostatic KdV equation (eq. (5.8)). To display the exact excitation patterns and their basic features, we numerically analyze equation (5.8) by the fourth-order Runge–Kutta (RK-

IV) method in judicious plasma conditions [1]. The obtained numerical profiles are shown in figure 5.2. Moreover, figure 5.3 shows their relevant conserved quantities graphically. Figure 5.2 shows the spatial profiles of the normalized lowest-order perturbed electrostatic (a) potential, (b) field, (c) potential curvature, and (d) phase portrait. Various lines correspond to Case (1): $m_d = 2.741\times10^{-12}$ kg (blue line), Case (2): $m_d = 2.754\times10^{-12}$ kg (red line), Case (3): $m_d = 2.768\times10^{-12}$ kg (green line), and Case (4): $m_d = 2.781\times10^{-12}$ kg (black line), respectively. Different input sensitive initial values used in the simulation are $(\Phi)_i = 1.418\times10^{-6}$, $(\Phi_\rho)_i = 1.00\times10^{-5}$, and $(\Phi_{\rho\rho})_i = 4.40\times10^{-3}$. The other parameters kept fixed in our scheme are $M_{eo} = 1.00\times10^{-2}$, $M_{io} = 1.00\times10^{-3}$, $M_{dno} = 0.67$, $M_{dco} = 1.00\times10^{-3}$, $Z_d = 1.00\times10^{2}$, $n_{eo} = 6.50\times10^{6}$ m^{-3}, $n_{io} = 9.03\times10^{8}$ m^{-3}, and $n_{dno} = 2.51\times10^{4}$ m^{-3}. Here, the lowest-order perturbed electrostatic potential (Figure 5.2(a)) undergoes a new type of dynamic transition from solition-chain to a single flat compressive soliton pattern (extended) with slight increase in dust grain mass. In the HII region with $T_p = 1$ eV, $\in = 10^{-2}$, and $\lambda_J = 3.09\times10^{8}$ m [1, 4] the average strength of the electrostatic potential fluctuations is $\Phi_1 \sim 10^{-3}$, which is physically $\phi_{phys} = \in (T_p \Phi_1 / e) \sim 10^{-5}$ V. The corresponding field fluctuations (Figure 5.2(b)) are hybrid periodic waves composed of both soliton (compressive) and antisoliton (rarefactive) counterparts in accordance with the basic law of conservative dynamics $(E_{e1} = -\nabla\Phi_1)$. The real strength of the electric field fluctuations is $E_{ephys} = \in (T_p E_{e1} / e\lambda_J) \sim 3.23\times10^{-14}$ V m^{-1}. The curvature profile (Figure 5.2(c)) shows that the degree of deviation from quasi-neutrality mapped over the cloud equilibrium is irregular, which is contributed by soliton-trains of varying amplitudes. The real magnitude of the potential curvature is $(\partial_{xx}\phi)_{phys} = \in (T_p \partial_{\rho\rho}\Phi_1 / e\lambda_J^2) \sim 1.04\times10^{-25}$ V m^{-2}. This is a very small quantity signifying that the global quasi-neutrality is not affected appreciably due to the inertia-based perturbation treatment amidst considered weak nonlinearities. The phase portrait (Figure 5.2(d)) gives a parametric representation of the geometrical trajectories for the global behavior of local fluctuation dynamics in the phase plane. This reveals a conservative nature as the trajectories evolve as closed-form structures. For increasing m_d, the trajectories overlap over one another at the potential value corresponding to that near the cloud center. Therefore, it is pertinent to add that the central portion of the cloud surrounds the most stable fixed point. The trajectories in the phase portraits start to

get slightly separated from one another as the perturbed potential increases in magnitude from the center outwards. This reveals that the cloud gets gradually more unstable at spatial points away from the cloud center with an increase in m_d .

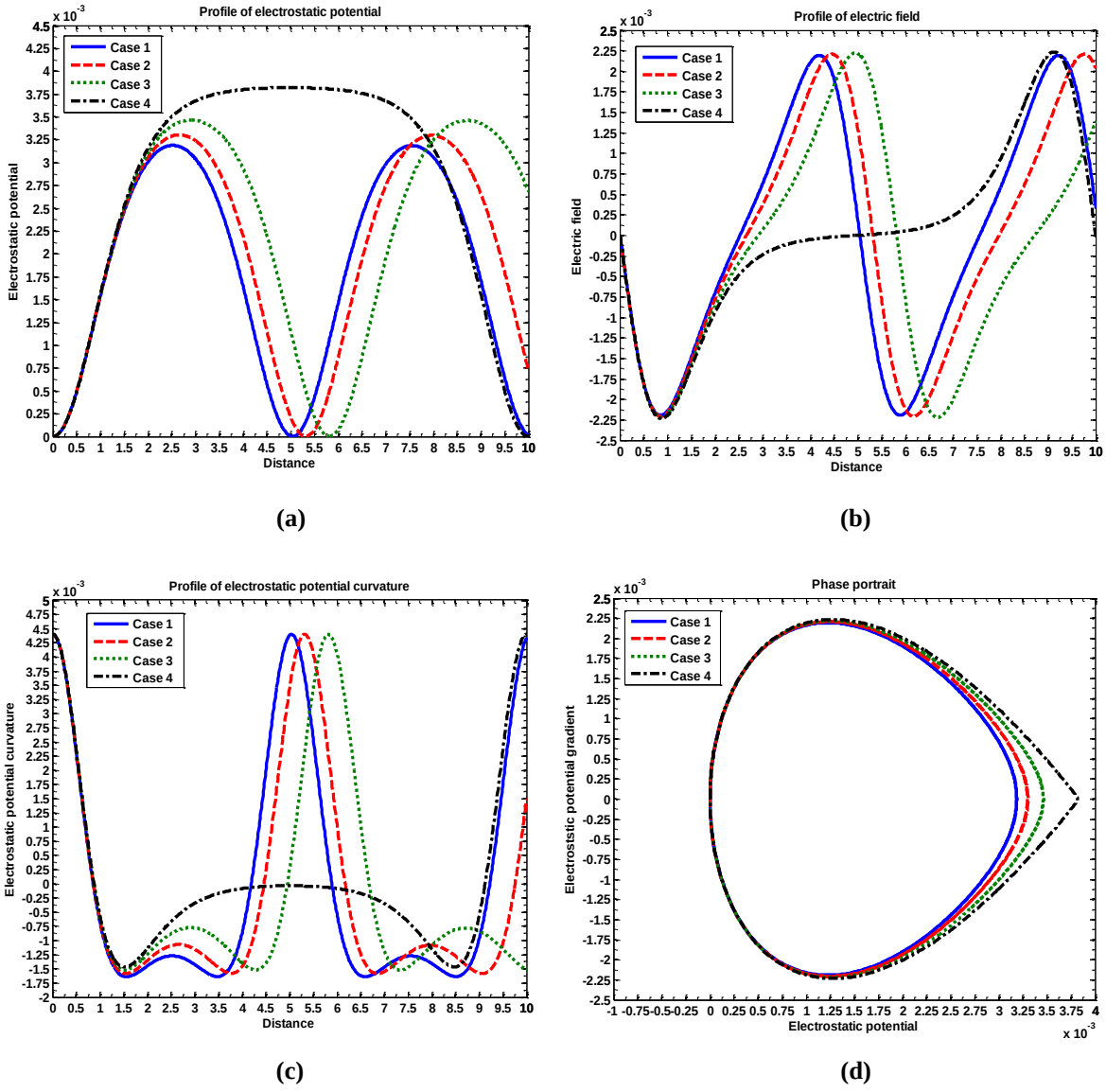

Figure 5.2 *Profile of the normalized lowest-order perturbed electrostatic (a) potential, (b) field, (c) potential curvature, and (d) phase portrait. Various lines correspond to Case (1):* $m_d = 2.741 \times 10^{-12}$ *kg (blue line), Case (2):* $m_d = 2.754 \times 10^{-12}$ *kg (red line), Case (3):* $m_d = 2.768 \times 10^{-12}$ *kg (green line), and Case (4):* $m_d = 2.781 \times 10^{-12}$ *kg (black line), respectively. Various input and initial parameter values are given in the text.*

Figure 5.3 shows the evolutionary patterns of the first five conserved quantities of electrostatic KdV dynamics under the same condition as figure 5.2. Different lines correspond to Case (1): P_{e1} (blue line), Case (2): P_{e2} (red line, rescaled by dividing with 2.00×10^{-3}), Case (3): P_{e3} (green line, rescaled by dividing with 2.20×10^{-3}), Case (4): P_{e4} (black line, rescaled by dividing with 7.14×10^{-6}), and Case (5): P_{e5} (pink line, rescaled by dividing with 2.50×10^{-8}). The first conserved quantity, as usual mass density (blue line) of the KdV dynamics [13], evolves as soliton-like structure with physical value $P_{e1phy} \sim\in P_{e1} = 10^{-5}$ V. Again, the second conserved quantity, i.e., momentum density (red line) of the KdV dynamics also evolves as a two-tail soliton-like pattern with amplitude $P_{e2} \sim 10^{-6}$. Similarly, the third conserved quantity, i.e., energy density (green line) also appears as a soliton-like pattern with amplitude $P_{e3} \sim 10^{-6}$. The other higher-order conserved quantities are of great significance in applied mathematics only. They are physically soliton-type in patterns, as analyzed by many authors in past too [13-14]. Here too, the higher-order conserved quantities appear with some fluctuations and distortions due to the re-organization of internal convective flow dynamics of the massive grains and background acoustic spectral components tending to establish a new dynamical equilibrium subject to weakly nonlinear perturbation.

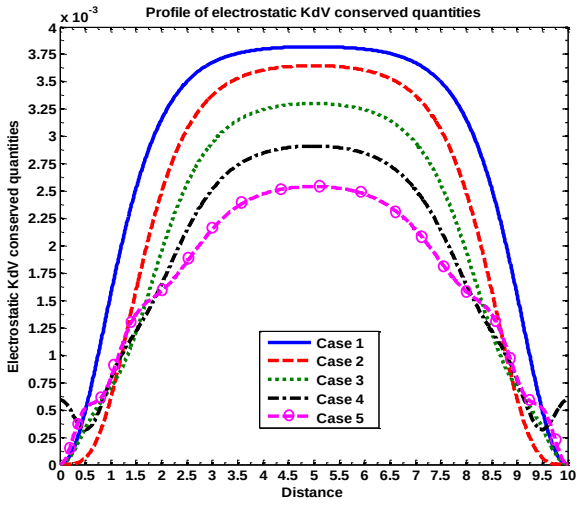

Figure 5.3 *Profile of the first five conserved quantities of electrostatic KdV dynamics under the same condition as figure 5.2. Various lines correspond to Case (1): P_{e1} (blue line), Case (2): P_{e2} (red line), Case (3): P_{e3} (green line), Case (4): P_{e4} (black line), and Case (5): P_{e5} (pink line).*

5.5.2 Self-gravitational Fluctuations

Similar to the electrostatic fluctuations, the nonlinear self-gravitational oscillation dynamics of the planar DMC too is collectively governed by KdV equation (eq. (5.13)) on the lowest-order perturbed self-gravitational potential. The equation is integrated numerically as before to examine the detailed features of the excitation patterns and their conservative dynamics in some realistic cloud conditions [1]. The numerical profiles thus obtained are presented in figures 5.4-5.5.

Figure 5.4 shows the spatial profile structures of the normalized lowest-order perturbed self-gravitational (a) potential, (b) field, (c) potential curvature, and (d) phase portrait. Various lines correspond to Case (1): $m_d = 4.30\times10^{-9}$ kg (blue line), Case (2): $m_d = 1.79\times10^{-8}$ kg (red line), Case (3): $m_d = 3.15\times10^{-8}$ kg (green line), and Case (4): $m_d = 4.50\times10^{-8}$ kg (black line), respectively. Different input initial values used here are $(\Psi)_i = 1.00\times10^{-8}$, $(\Psi_\rho)_i = 1.00\times10^{-7}$, and $(\Psi_{\rho\rho})_i = 8.90\times10^{-6}$. The other sensitive parameters kept fixed are $M_{eo} = 1.00\times10^{-3}$, $M_{io} = 1.00\times10^{-4}$, $M_{dno} = 0.10$, $M_{dco} = 1.00\times10^{-3}$, $Z_d = 100$, $n_{eo} = 6.50\times10^{7}$ m^{-3}, $n_{io} = 1.10\times10^{9}$, $n_{dno} = 2.50\times10^{4}$ m^{-3}, and $\mu = 1.00$. It shows that the fluctuations evolve as soliton-chain-like and soliton pattern (hump-like) of different characteristics (Figure 5.4(a)). The amplitude of the pattern increases with an increase in m_d, and vice versa. A unique transition from a soliton-chain to a single soliton structure (with two tails) is found to take place. This, in fact, goes well in accordance with the Newtonian gravitational law, revealing that the self-gravitational potential increases with the grain mass within the point mass approximation, and vice versa. In the HII region with $T_p \sim 1$ eV, $\in = 10^{-2}$, and $\lambda_J = 3.09\times10^{8}$ m [1, 4] the strength of the self-gravitational potential fluctuations is $\psi_{phys} = \in (T_p \Psi_1 / e) \sim 10^{-7}$ J C^{-1}. It is again seen that the self-gravitational field fluctuations of the cloud associated with the compressive soliton patterns is a nonlinear periodic wave composed of both compressive and rarefactive solitary counterparts (Figure 5.4(b)) with real strength $E_{gphys} = \in (T_p E_{g1} / e\lambda_J) \sim 3.23\times10^{-16}$ J C^{-1} m^{-1}. This is as per the basic law of the conservative self-gravitational KdV dynamics $(E_{g1} = -\nabla \Psi_1)$, such that the curvatures (Figure 5.4(c)) with physical strength $(\partial_{xx}\psi)_{phys} = \in (T_p \partial_{\rho\rho} \Psi_1 / e\lambda_J^2) \sim 1.04\times10^{-27}$ J C^{-1} m^{-2} get self-consistently reorganized in a like dynamical fashion. So, the nature of the phase portrait turns into bigger sizes, but are always closed in shape (Figure 5.4(d)). The phase portrait again reveals that the central portion of the

cloud surrounds the most stable fixed point and the stability of the cloud gradually decreases at spatial points away from the cloud center.

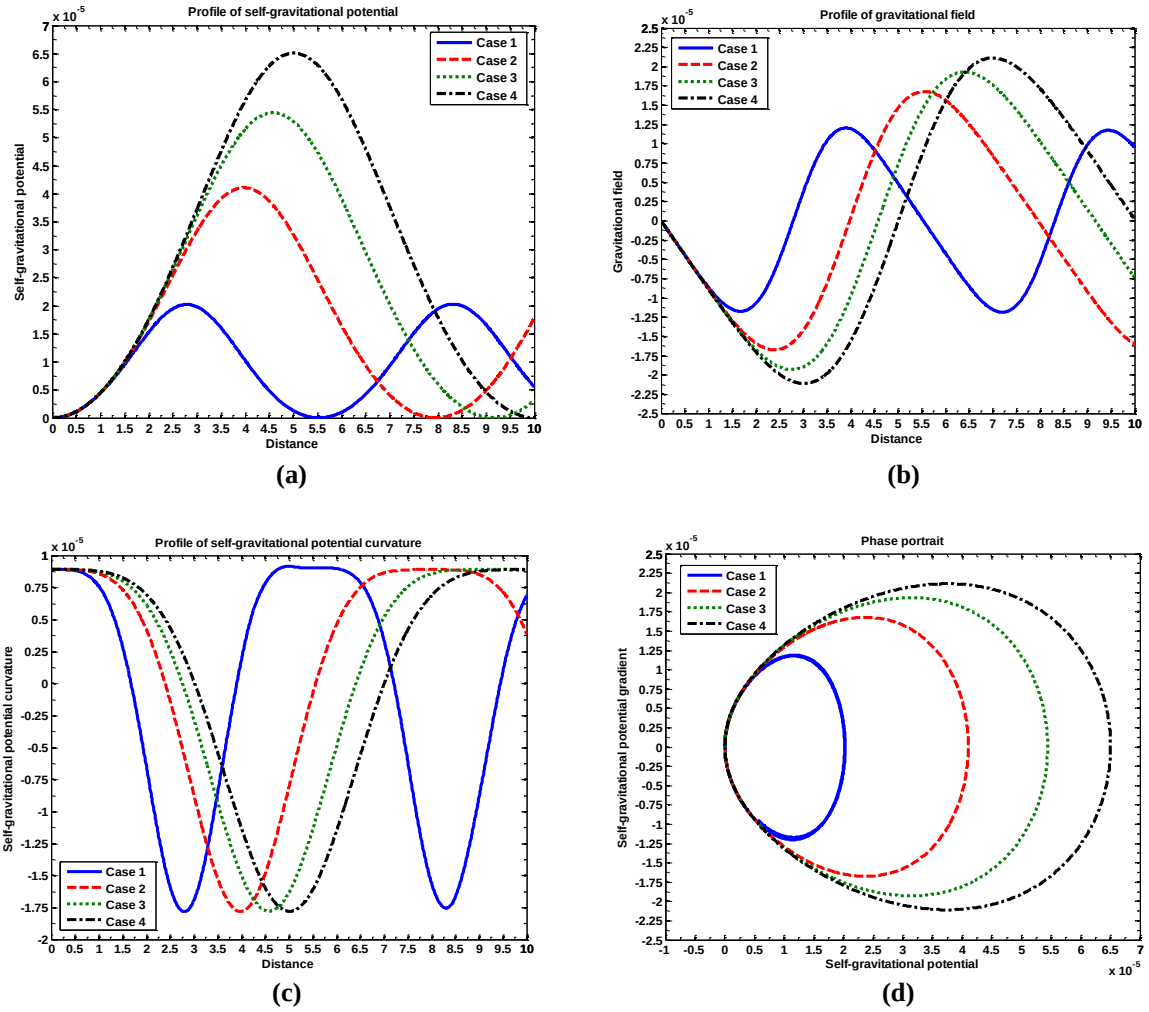

Figure 5.4 *Profile of the normalized lowest-order perturbed self-gravitational (a) potential, (b) field, (c) potential curvature, and (d) phase portrait. Various lines correspond to Case (1):* $m_d = 4.30\times10^{-9}$ *kg (blue line), Case (2):* $m_d = 1.79\times10^{-8}$ *kg (red line), Case (3):* $m_d = 3.15\times10^{-8}$ *kg (green line), and Case (4):* $m_d = 4.50\times10^{-8}$ *kg (black line), respectively. Various numerical input and initial parameter values are given in the text.*

Figure 5.5 gives the profile of the first five conserved quantities of self-gravitational KdV dynamics under the same condition as figure 5.4. Different lines correspond to Case (1): P_{g1} (blue

line), Case (2): P_{g2} (red line, rescaled by dividing with 4.00×10^{-5}), Case (3): P_{g3} (green line, rescaled by dividing with 4.00×10^{2}), Case (4): P_{g4} (black line, rescaled by dividing with 5.00×10^{-2}), and Case (5): P_{g5} (pink line, rescaled by dividing with 1.10×10^{-5}). The first conserved quantity, i.e., mass density (blue line) [13] of the self-gravitational KdV dynamics soliton evolves as two tail soliton-like structure with physical value $P_{g1phy} \sim\in P_{g1} \sim 10^{-7}$ J C^{-1}. Again the second conserved quantity, i.e., momentum density of the self-gravitational KdV dynamics evolves as soliton-like pattern with amplitude $P_{g2} \sim 10^{-9}$. Similarly, the third conserved quantity, i.e., energy density also appears as a soliton-like pattern with amplitude $P_{g3} \sim 10^{-3}$. The other higher-order conserved quantities are physically the derivative forms of the lowest-order ones, as analyzed by many authors elsewhere in past [13-14]. The higher-order conserved quantities appear with some background fluctuations and destabilizations due to the re-organization of internal convective flow dynamics and acoustic winds of the plasma constituents, thereby tending to achieve a new dynamical equilibrium amid weak perturbation.

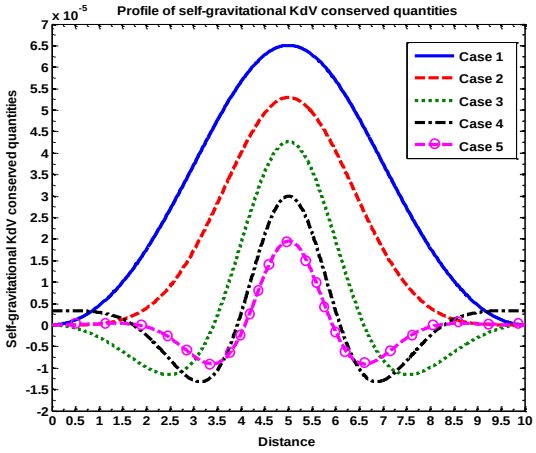

Figure 5.5 *Profile of the first five conserved quantities of self-gravitational KdV dynamics under the same condition as figure 5.4. Various lines correspond to Case (1):* P_{g1} *(blue line), Case (2):* P_{g2} *(red line), Case (3):* P_{g3} *(green line), Case (4):* P_{g4} *(black line), and Case (5):* P_{g5} *(pink line).*

5.5.3 Comparative Fluctuations

The nonlinear gravito-electrostatic fluctuations in a partially charged self-gravitating DMC, within the framework of the Jeans homogenization assumption, governed by a unique pair of KdV

equations. Coexcitation of some solitary patterns are found as due basically to the intermittent interplay between the self-gravitational dispersion (due to massive grains) and hydrodynamic nonlinearity (due to hydrodynamicity). Although the excitation mechanisms are similar, the obtained spectral classes of the eigenmodes have some distinctive features between them in terms of response characteristics. The ratio between electrostatic-to-self-gravitational fluctuations is obtained as $\phi_{phys}/\psi_{phys} \approx E_{ephys}/E_{gphys} \approx (\partial_{xx}\phi)_{phys}/(\partial_{xx}\psi)_{phys} \sim 10^2$. Thus, the electrostatic fluctuations are more dominant (due to all charged particles) than the corresponding self-gravitational counterparts (due to all massive particles) in the DMC. Besides, the ratio of first conserved quantity of electrostatic and self-gravitational KdV dynamics is $P_{e1phy}/P_{g1phy} \sim 10^2$. A quantitative glimpse on the various nonlinear electrostatic (Figures 5.2-5.3) and self-gravitational (Figures 5.4-5.5) eigenmode structures along with their relative conserved quantities, exhibiting some distinctive features are presented in Table 5.1.

Table 5.1: Electrostatic and self-gravitational fluctuations

No.	Items	Electrostatic	Self-gravitational
1	Initial assumption	Quasi-neutrality	Jeans mass-neutrality
2	Source	All Coulombic particles	All Newtonian particles
3	Origin of dispersion	Quasi-neutrality deviancy	Self-gravity
4	Origin of nonlinearity	Hydrodynamic convection	Same
5	Evolution equation	Electrostatic KdV	Self-gravitational KdV
6	Eigenmode structure	Compressive soliton-chain and flattened soliton patterns	Double-tail soliton (hump) and soliton-chain patterns
7	Eigenmode amplitude	Small ($\sim 10^{-5}$ V)	Smaller ($\sim 10^{-7}$ J C^{-1})
8	Field amplitude	Small ($\sim 3.23\times10^{-14}$ V m^{-1})	Smaller ($\sim 3.23\times10^{-16}$ J C^{-1} m^{-1})
9	Geometrical curvature	Low ($\sim 1.04\times10^{-25}$ V m^{-2})	Lower ($\sim 1.04\times10^{-27}$ J C^{-1} m^{-2})
10	Functional form	$\Phi_1(\rho) = \Phi_{1m}\sec h^2(\rho/\omega_e)$	$\Psi_1(\rho) = \Psi_{1m}\sec h^2(\rho/\omega_g)$
11	Effect of increasing m_d	Amplitude of fluctuations increases (slowly)	Amplitude of fluctuations increases (rapidly)
12	Effect of increasing q_d (Plots in Ref. [17])	Amplitude decreases (very slow)	Amplitude increases (fast)

13	Effect of increasing μ (Plots in Ref. [17])	Amplitude rises, and shows a shape transition (soliton-chain to soliton)	Amplitude decreases and no structural transition is noticed
14	Effect of increasing n_{io} (Plots in Ref. [17])	Amplitude slightly increases, and results in a transition from soliton-chain to extended soliton	Amplitude falls (fast), and results in a transition from single soliton (two-tail, hump-like) to soliton-chain
15	Effect of increasing n_{eo} (Plots in Ref. [17])	Amplitude of fluctuation remains the same, but width rises (compacton)	Both amplitude and width decreases very slowly
16	Normal field shape	Hybrid multi-peakon of soliton (compressive) and antisoliton (rarefactive)	Similar (but, with no multi-peakon characteristics)
17	Usual curvature shape	Amalgam of compressive and rarefactive structures	Similar (with valley-like soliton and soliton-train)
18	Normal shape transition	Soliton-chain to flat soliton, and vice versa	Soliton to soliton-chain, and vice versa
19	Phase portraits	Closed and the center is the most stable fixed point	Same (conservative)
20	Shape of conserved soliton mass density	Flat soliton-like pattern	Two-tail soliton-like pattern
21	Shape of conserved soliton momentum density	Two-tail soliton-like pattern	Soliton-like pattern
22	Shape of conserved soliton energy density	Soliton-like pattern	Soliton-like pattern
23	Validity limit	Weak nonlinearity (< 3rd order) and nonrelativistic point-charge assumption	Same, but for nonrelativistic point-mass estimate

5.6 CONCLUSION

In this chapter, an inertia-based theoretical model is developed to study the gravito-electrostatic pulsational mode stability in a planar self-gravitaying DMC on astrophysical scale. The basis of the adopted model is the Jeans assumption of self-gravitating homogeneous uniform medium paving the way for local analytical simplification. The active inertial role of the cloud thermal species and weak frictional coupling are included. The model supports the excitation, existence and evolution of the nonlinear gravito-electrostatic eigenmodes in the form of diverse solitary spectral patterns. The observed wide-range spectrum of the eigenmodes include flattened soliton, extended soliton, and soliton-chain altogether collectively known as soliton-patterns. Their dynamic structures are governed by a pair KdV equation in modified form developed by applying a standard multiscale analysis. This is observed that the electrostatic eigenmodes have greater strengths as compared with those of the self-gravitational ones ($\phi_{phy}/\psi_{phy} \sim 10^2$). The corresponding unipolar self-gravitational contribution is not so strong because of small inertial masses of the constituents unless and until the long-rang force-ratio condition $F_g/F_e = Gm_d^2/q_d^2 \sim 0(1)$ is fulfilled to form gravito-electrostatically confined equilibrium diverse astrophysical structures [1]. The closed form of phase portraits reveal that the intrinsic conservative dynamics involved in the KdV system is well-satisfied even in the presence of the lowest-order inertial correction of thermal species and weak friction.

The analysis of the primary conserved quantities for both electrostatic and self-gravitational KdV dynamics together with their constructed shapes is also presented in this chapter. Different conservative forms of the gravito-electrostatic fluctuations are analytically derived to show the basic conserved densities and associated fluxes pictorially. The evolution patterns of the conserved mass density, momentum density, and energy density are elaborately discussed. They retain the average shape of solitary structures, but in a slightly distorted form for their higher ranks. It is interesting to note that the pulsational mode fluctuations in our inhomogeneous cloud configuration dynamically evolve in such a way that all these derived explicit forms of conservative properties remain conserved throughout their propagation on the astrophysical scales of space and time. However, the next higher-order conserved densities show some fluctuations in their shapes because of background acoustic spectral winds. The underlying basis of nonlinear coupling of the diverse spectral components may put a platform for further investigation with great

significance in applied mathematics [13-14]. The detailed analyses of the analytical and numerical findings due to sensitive multi-parameter variations are elaborately discussed in the Ref. [17-18]. The solitary spectral patterns analyzed in our inertia-centric cloud model have astrophysical importance too. They are in partial and qualitative correspondence with the predictions on astrophysical nonlinear waves made by various spacecraft instrumentations, on-board multispace satellite reports, and experimental findings [3, 6, 19]. Examples of such clouds are *Lynds 204 Complex*, *Barnard 68*, and so forth. The methodological analysis may also be extensively applied to study the observed data on the dynamics of jets and associated bow shocks on the galactic scales as observed in certain galaxies like M51, NGC 1068, NGC 5258, Circinus, Mrk 673, and so forth.

Our investigation may afford different and wider scopes for elaborate improvement and refinements to understand the temporal eigenmode evolution with various equilibrium spatio-temporal inhomogeneities. For a realistic and creative study, our model needs a number of refinements. It must include grain rotations, magnetic field, dust charge fluctuations, viscosity, grain-size distribution, diffusion, etc. [1-7, 10-11]. Although simplified, we hope that the obtained results may be applied as vibrant elements to perceive some realistic space, stellar, and astrophysical plasma environments, and their associated wave kinetics having non-trivial roles in diverse bounded structure formation mechanisms.

REFERENCES

1. Dwivedi, C. B., et al. Pulsational mode of gravitational collapse and its impact on the star formation, *Astron. Astrophys.* **345**, 1049-1053, 1999.
2. Klessen, R. S., et al. Numerical star-formation studies-A status report, *Adv. Sci. Letts.* **4**, 258-285, 2011.
3. Verheest, F. Waves and instabilities in dusty space plasmas, *Space Science Reviews* **77**, 267-302, 1996.
4. Spitzer, L., Jr. *Physical Processes in the Interstellar Medium*, WILEY-VCH Verlag GmbH & Co. KGaA, Weinheim, 2004.
5. Adams, F. C., et al. General analytical results for nonlinear waves and solitons in molecular clouds. *Astrophys. J.* **426**, 629-645, 1994.
6. Watkins, R., et al. Nonlinear waves and solitons in molecular Clouds, in *The Physics and Chemistry of Interstellar Molecular Clouds,* Proceedings of the 2nd Cologne–Zermatt

Symposium Held at Zermatt. Switzerland, 21–24 September 1993, G. Winnewisser, & G. C. Pelz, eds., Springer, New York, 1995, 115-117.

7. Shukla, P. K. and Mamun, A. A. Fragmentation instability of molecular clouds, *Phys. Lett. A.* **271**, 402-406, 2000.
8. Mamun, A. A. and Shukla, P. K. Instabilities of self-gravitating dusty clouds in magnetized plasmas, *Phys. Plasmas*. **7**, 3762-3770, 2000.
9. Karmakar, P. K. Application of inertia-induced excitation theory for nonlinear acoustic modes in a colloidal plasma equilibrium flow, *Pramana – J. Phys.* **68**, 631-648. 2007.
10. Chiuderi, C. & Velli, M. *Physics of Plasma Astrophysics,* Springer, Italia, 2015.
11. Bliokh, P., et al. *Dusty and Self-gravitational Plasmas in Space*, Kluwer academic publisher, London, 1995.
12. Deka, U. and Dwivedi, C. B. Effect of electron inertial delay on Debye sheath formation, *Braz. J. Phys*. **40**, 333-339, 2010.
13. Miura, R. M., et al. Kortewegde Vries equation and generalizations. II. Existence of conservation laws and constants of motion, *J. Math. Phys.* **9**, 1204-1209, 1968.
14. Ali, A. and Kalisch, H. On the formulation of mass, momentum and energy Conservation in the KdV equation, *Acta Appl. Math.* **133**, 113-131, 2014.
15. Cadez, V. M. Applicability problem of Jeans criterion to a stationary self-gravitating cloud, *Astron. Astrophys.* **235**, 242-244, 1990.
16. Asano, N. Wave propagations in non-uniform media, *Suppl. Prog. Theor. Phys*. **55**, 52-79, 1974.
17. Karmakar, P. K. and Borah, B. Inertia-centric stability analysis of a planar uniform dust molecular cloud with weak neutral-charged dust frictional coupling, *Plasma Science and Technology* **16**, 433-447, 2014.
18. Borah, B. and Karmakar, P. K. Pulsational mode fluctuations and their basic conservation laws, *Adv. Space Res.* **55**, 416-417, 2015.
19. Ergun, R. E. et al. FAST satellite observation of large-amplitude solitary structure, *Geophys. Res. Lett.* **25**, 2041-2044, 1998.